Theoretical site- and symmetry-resolved density of states and experimental EELS near-edge spectra of AlB_2 and TiB_2

K. Lie and R. Høier
Department of Physics, Norwegian University of Science and Technology (NTNU), N-7034 Trondheim, Norway

R. Brydson
Department of Materials, School of Process, Environmental and Materials Engineering, University of Leeds, Leeds LS2 9JT, United Kingdom

(Received 29 June 1999)

We report the orientation dependent B *K*-edge electron-loss near-edge spectroscopy spectra of the isostructural compounds AlB_2 and TiB_2. The observed differences between the experimental spectra of the borides are discussed in terms of the variation in bonding between the two materials. The orientation dependence is rationalized in terms of the anisotropic nature of the common crystal structure. For a detailed comparison with experiment, we have employed a first-principles method for the calculation of the partial density of states. This method is based on band calculations using the full-potential linearized augmented plane-wave method within density-functional theory. We ascribe the origin of the discrepancies between the broadened ground-state density of states and experiment to the presence of a core hole in the final state. The core-hole effect is self-consistently accounted for via the use of *ab initio* supercell calculations, leading to improved agreement with experiment particular in certain crystallographic directions, where screening of the core hole is expected to be much reduced. Additionally a detailed analysis of the valence-band structure, charge-transfer effects, and covalency in the diborides has been undertaken.

I. INTRODUCTION

Electron-energy-loss spectroscopy (EELS) has rapidly become a well-established technique for studying the unoccupied electronic states of solids.[1] In EELS and, in particular, in electron-loss near-edge spectroscopy (ELNES), an electron is excited from an atomiclike core level into a previously unoccupied bandlike electronic state above the Fermi level E_F. This is a local process obeying the dipole selection rules and, because of the atomiclike character of the core orbital, EELS spectra are considered to be directly proportional to the site and symmetry projected unoccupied electronic density of states (DOS). This provides the basis for a direct comparison with the results of theoretical band-structure calculations. However, the influence of the core hole produced during the EELS excitation process makes the relationship between the ground-state partial density of states and the ELNES spectra less direct. The core hole is known to distort the local density of states around the core-ionized site, and the effects may be very complex in an interacting-electron system.[2] In systems with narrow conduction bands, as in $L_{2,3}$ $(2p)$ edges of many transition-metal compounds and in the $M_{4,5}$ edges of rare earths, the spectra are characterized by the presence of sharp features (white lines), satellites, and large multiplet effects.[3,4] We note that an understanding of core-hole effects is important not only for EELS studies of unoccupied electronic states, but in all techniques involving creation and annihilation of core holes. Examples of such techniques are near-edge and extended x-ray-absorption fine structure, Auger spectroscopy, photoemission, and x-ray emission.

In this paper we investigate the influence of the core hole on the measured B *K*-edge spectra of AlB_2 and TiB_2, by comparing the experimental EELS results with the results of state-of-the-art band-structure calculations. The original motivation for the present work was to gain a better understanding of the EELS spectra of TiB_2, which was studied in previous papers.[5,6] The fact that AlB_2 and TiB_2 are isostructural makes these diborides an ideal system to study the effects of the transition-metal $3d$ electrons. Both borides adopt a layered, hexagonal structure $(P6/mmm)$ with alternating hexagonal sheets of metal and boron atoms, respectively, arranged perpendicularly to the *c* direction. Table I gives the crystallographic parameters and the atomic configurations for the two diborides. An investigation of the electronic structure, both occupied and unoccupied, states of these diborides has both fundamental scientific and technological

TABLE I. Crystallographic parameters and atomic configurations. *X*-B and B-B denote distances between neighboring atoms.

Compound	a (Å)	c (Å)	$\frac{c}{a}$	*X*-B (Å)	B-B (Å)	Atomic configuration
AlB_2	3.005	3.253	1.083	2.378	1.735	Al $3s^2 3p^1$; B $2s^2 2p^1$
TiB_2	3.030	3.230	1.066	2.381	1.750	Ti $3d^2 4s^2$; B $2s^2 2p^1$

significance. The AlB_2-type structure is one that is adopted by many of the transition-metal diborides TB_2 (T=Sc, Ti, V, Cr, Mn, Y, Zr, Nb, Mo, Hf, Ta), and they possess some unique properties such as high melting point, hardness, chemical stability, and metallic properties.[7] A simple ionic picture has often been adopted for TB_2 compounds.[8] According to this picture, the transition metal donates one electron to each boron atom, resulting in a graphitelike two-dimensional net. The remaining free electrons on the metal would then account for the metallic conductivity exhibited by many of these materials. This purely electrostatic image of bonding has been challenged, however, by recent calculations,[5,9,10] showing that Ti-B covalent bonding is very important in the electronic structure, and therefore, in influencing the physical properties of TiB_2. In this work we have performed site- and symmetry-resolved unoccupied density-of-states calculations, which have proven to give reliable results well above the bottom of the conduction band when compared with experiment. In Secs. II A and II B, we show the results of the calculated ground-state and excited state DOS, respectively. In Sec. III we compare the experiments with the calculated DOS, both with and without the inclusion of the core hole, and we identify the effects of the core-hole potential on the measured spectral functions.

II. METHODS: DETAILS OF EXPERIMENT AND CALCULATIONS

A. Experimental details

EEL spectra were collected using a parallel recording Gatan 666 spectrometer fitted to a Phillips CM 30 transmission electron microscope (LaB_6 source) operating at a nominal voltage of 200 kV. The spectra were obtained with an energy dispersion of 0.05 eV/channel, convergence angle $\alpha=3.0$ mrad, and a collection angle $\beta=1.5$ mrad. The B K edges were acquired in diffraction mode (image coupling) with a 100-μm condenser aperture. The energy resolution [measured as the full width at half maximum (FWHM) at the zero-loss peak] was typically around 1.1 eV. With the parameters listed above, the characteristic angle θ_E was 0.7 mrad. In this situation the collection angle is about $2\theta_E$, and is small compared to the crossover in the weighting of the two momentum-resolved components parallel and perpendicular to the electron-beam direction, which occurs at about $8\theta_E$. This implies that there is good resolution of the two directional components, and that, under all experimental conditions the momentum transfer parallel to the beam is the dominant factor. For the experimental conditions there is a convergent beam ($\alpha=3$ mrad), but for small scattering angles the relationship between the two components is only slightly modified.[11]

The processing of the sintered TiB_2 ceramic is described elsewhere;[12] however, the polycrystalline nature of this sample permits a large range of specimen orientations to be studied with limited tilting. The AlB_2 phase was studied in an Al-3% B alloy (7258), which consisted of large plate-shaped AlB_2 particles (typical size between 5 and 10 μm) distributed in an aluminum matrix. Thin specimens were prepared by low angle ion-milling and energy-loss measurements were carried out soon after thin foil preparation to minimize any possible oxidation effects. This proved to be very important, as even a small oxidation layer of boron oxide or metal borate distorts the measured B K-edge spectrum.

Spectra from areas showing negligible oxygen contents (<5 atom %) and of similar thickness ($t/\lambda=0.5$), as measured relative to the total inelastic mean free path of the 200-keV electrons (λ), were compared when the orientation dependency was analyzed. The absolute energy scale was referenced to the first peak in the TiB_2 B K-edge ELNES which was set to 188.6 eV as observed in isostructural CrB_2.[13] Spectra were acquired parallel and normal to the unit cell c axes (as determined by electron diffraction). Further spectra were acquired near but not exactly on the particular zone axis, when near-edge features were analyzed; however, no significant channeling effects could be detected. Spectra were deconvoluted using the Fourier-ratio[14] method, as the low loss contribution from the same area was measured separately.

The dark current due to the photodiode array was subtracted from the spectra. Gain variations were corrected for by acquiring several spectra (8–15) at different positions on the photodiode array, and averaging them to produce a gain corrected spectrum as described by Boothroyd, Sato, and Yamada.[15] This approach permits the use of a shorter integration time (1 sec), which is required to improve energy resolution, while still having a good signal-to-noise ratio. The continuum background before the edge was fitted and subtracted using the standard power-law procedure.[14]

B. Electronic structure calculations

Theoretical calculations were performed using the full potential linearized augmented plane-wave method (LAPW) as embodied in the WIEN97 code[16] in a scalar relativistic version without spin-orbit coupling, which is one of the most accurate schemes for electronic structure calculations in solids. In the LAPW method, the unit cell is divided into two parts: atomic spheres centered on the atomic sites (with atomic sphere radii R_{mt} of 2.0 and 1.6 a.u. for Al/Ti and B, respectively) and an interstitial region. Inside the atomic spheres, the basis set used to describe electronic states employs atomiclike functions, while in the interstitial region plane waves are used. Exchange and correlation effects are treated within density functional theory, using the common local-spin-density approximation. The linearization alone in the LAPW method is reliable for about 1–2 Ry above the Fermi level. For TiB_2, a local orbital extension was used to improve the situation for states high above E_F. The initial basis set included $4s$, $4p$, and $3d$ functions at the Ti sites in addition to local orbitals for semicore $3s$ and $3p$ and $2s$ and $2p$ functions were used at the B site. After self-consistency was achieved for this basis set, we included a few high-energy local orbitals; $4d$-like functions were added at the Ti site, while $3s$- and $3p$-like functions were added at the B site. In addition to this expansion, we also tried to increase the Ti $4s$ and $4p$ energies by 1 Ry. With this improved basis set a few more self-consistency cycles were performed. The charge density and potentials were expanded into spherical harmonics up to $l=12$ inside the spheres, and the Brillouin-zone integration was performed using a modified tetrahedron method[17] using 140 special **k** points in the irreducible wedge.

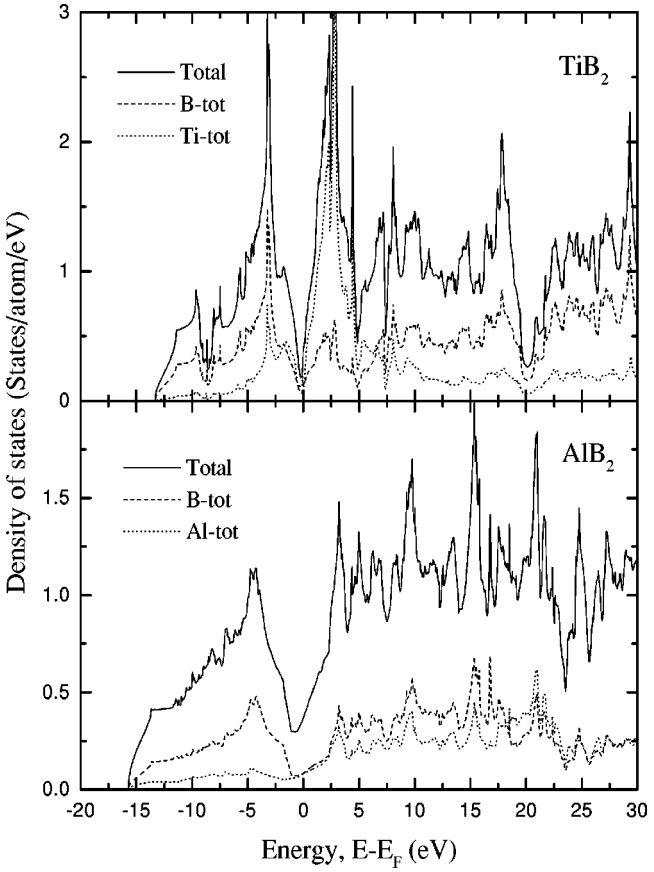

FIG. 1. Comparison of the total- and site-resolved (ground state) density of states of the two diborides studied. Note the main difference arises from the Ti $3d$ states in the transition-metal diboride in the interval from -5 to 5 eV. However, both diborides show a pseudogap at the Fermi energy.

Electron energy loss near-edge structure provides information about the unoccupied part of the band above the Fermi energy (E_F). The differential cross section for scattering as derived from Fermi's golden rule[1] is, within the dipole approximation, proportional to

$$\frac{d\sigma}{dE} \propto \{|m_{L+1}|^2 \rho_{L+1}(E) + |m_{L-1}|^2 \rho_{L-1}(E)\},$$

$$m_{L\pm1} = \langle f_{L\pm1}|r|i_L\rangle. \tag{1}$$

Here ρ is the density of unoccupied states with angular momentum $L\pm1$, $|i\rangle$ represents the initial inner-shell electron wave function, and $|f\rangle$ represents the final unoccupied state. It can be seen from Eq. (1) that the near-edge structure can be related to the local angular-momentum-resolved DOS projected onto the atomic site in question. This means that a K $(1s)$ shell excitation provides information about the unoccupied p DOS. More specifically in a uniaxial system such as the AlB_2 structure $\mathbf{q}\perp\mathbf{c}$ is proportional to p_x+p_y, while $\mathbf{q}\|c$ is proportional to p_z.

In this paper our interest will be focused on a description of localized excitations, in the context of which a core hole is present in the final state. The theoretical investigations presented here consist of ''heavy'' first-principles electronic structure calculations, with no variable parameters. In order to investigate theoretically the influence of the core hole created during the ELNES excitation process, we have performed supercell calculations where the excited atom is formally treated as an impurity. Two different models to describe the excited state were considered. First, for one of the atoms in the cell we omitted one of the electrons in the $1s$ orbital, while the number of electrons in the valence band was increased by one (this approach will later be referred to as the core-excited approach). This procedure simulates the experimental situation, in which the sample can easily supply an electron to screen a localized charge produced by the core hole. Such an approach allows in a natural way for the symmetry breaking of the system, and self-consistently describes the charge redistribution induced by the core hole. In the second approach we have employed the more widely used $Z+1$ approximation,[18] where the core hole is simulated as an extra nuclear charge at the excited atomic site. In this study of XB_2 $(X=\mathrm{Al,Ti})$, the supercell containing the core hole contained 16 B and eight X atoms, i.e., it was eight times larger than the unit cell $(2\times2\times2)$. The size of the supercell is important, and ultimately it should be large enough to inhibit interaction between excited atoms in neighboring supercells. Finally, the symmetry resolved DOS obtained on a core-ionized site was used to calculate the theoretical B K-edge ELNES spectrum.

TABLE II. Comparison of the nearest-neighbor (NN) distances in the diborides with that of hexagonal boron nitride and graphite. The chemical bonding in the hexagonal network for the latter two cases is known to consist of a combination of both σ and π bonding.

Compound	NN	NN (Å)
AlB_2	B-B	1.735
TiB_2	B-B	1.750
h-BN	B-N	1.446
graphite	C-C	1.420

In addition to the band-structure calculations described above, we have also performed multiple-scattering (MS) calculations.[19,20] MS theory is based on the interference between the outgoing electron wave of the ejected electron and the electron wave which has been backscattered from the atoms surrounding the excited atom. The scattering properties of the various atoms are described by phase shifts which are calculated non-self-consistently using a muffin-tin form for the potential. This is a common choice in which a constant potential is assumed in the interstitial region. This form of the muffin-tin approximation is best for close-packed structures,[21] and its spherical approximation inside the muffin tins is shown to be a poor approximation for the directional bonding in TiB_2 between Ti and B sites. In the limit of large cluster size the MS approach it is equivalent to Kohn-Korringa-Rostocker band theory. Since MS calculations are performed in real space, using a cluster approach, it is more easily applied to nonperiodic structures, such as interphases, grain boundaries, or systems with large unit cells. The muffin-tin radius was chosen to be half the nearest-neighbor distance within the various sheets, $R_{MT}=2.79$ a.u. for Ti and Al, and 1.65 a.u. for B. We have used the $X\alpha$ exchange

TABLE III. Angular decomposition of the LAPW valence charge in the muffin-tin spheres for titanium and aluminum diboride. *I* is the charge in the interstitial region (divided by eight for the supercells, describing the excited states, to allow comparison between ground and excited states). ''Σ at.den.'' is the superposition of neutral atomic densities. *G* state are the values for the fully self-consistent calculations. Bexc and B($Z+1$) are values for the calculation including a core-hole described by the core-excited and ($Z+1$) approximations, respectively. No significant intersite charge transfer between the two compounds could be detected.

TiB_2	Ti *s*	Ti *p*	Ti *d*	Ti tot	B *s*	B p_z	B p_{xy}	B tot	*I*
G state	2.058	5.907	1.627	19.61	0.538	0.366	0.706	3.644	5.107
Σ at.den.				19.85				3.54	5.07
Bexc.	2.06	5.90	1.64	19.61	0.74	0.60	1.20	3.59	5.12
B($Z+1$)	2.06	5.90	1.60	19.63	0.90	0.59	1.18	4.69	5.07
AlB_2	Al *s*	Al *p*	Al *d*	Al tot	B *s*	B p_z	B p_{xy}	B tot	*I*
G state	0.389	6.387	0.139	10.93	0.528	0.384	0.704	3.652	4.771
Σ at.den.				11.21				3.51	4.77
Bexc.	0.40	6.38	0.14	10.93	0.74	0.61	1.22	3.60	4.80
B($Z+1$)	0.40	6.40	0.14	10.93	0.91	0.59	1.18	4.70	4.77

potential,[22] with $\alpha=0.8$ in both cases. The computer program we used was that of Durham, Pendry, and Hodges.[19]

III. RESULTS AND INTERPRETATION

A. Comparison of the ground-state DOS of AlB_2 and TiB_2: Effects of Ti *d* states

In our previous paper[5] the electronic structure of TiB_2 was discussed. Three principal subbands, made up of B 2*s* states, B 2*s* and 2*p* and Ti 3*d* and 4*s* states, and Ti 3*d* and 4*s* states, respectively, could be differentiated in the TiB_2 valence band. Similar band-structure results for TiB_2 and other transition-metal (TM) diborides, using different theoretical methods, were noted by several authors.[9,10,23–27] A common feature for all TM diborides and AlB_2 is the deep DOS minimum (pseudogap) at the Fermi energy separating the valence band and the conduction band. According to Pasturel *et al.*,[28] a pseudogap arises because of a strong chemical interaction. The *M*-B covalent bonding is believed to be responsible for this effect. In Fig. 1 we compare the total DOS for AlB_2 and TiB_2. In both systems we observe a deep minimum in the DOS at the Fermi energy, although this gap appears much broader in the case of AlB_2. The Ti 3*d* states in TiB_2 are the dominant features in the interval from -5 to 5 eV, responsible for this difference. These tightly bound states show overlap with B 2*p* and to a lesser extent B 2*s* states in this narrow energy interval both above and below

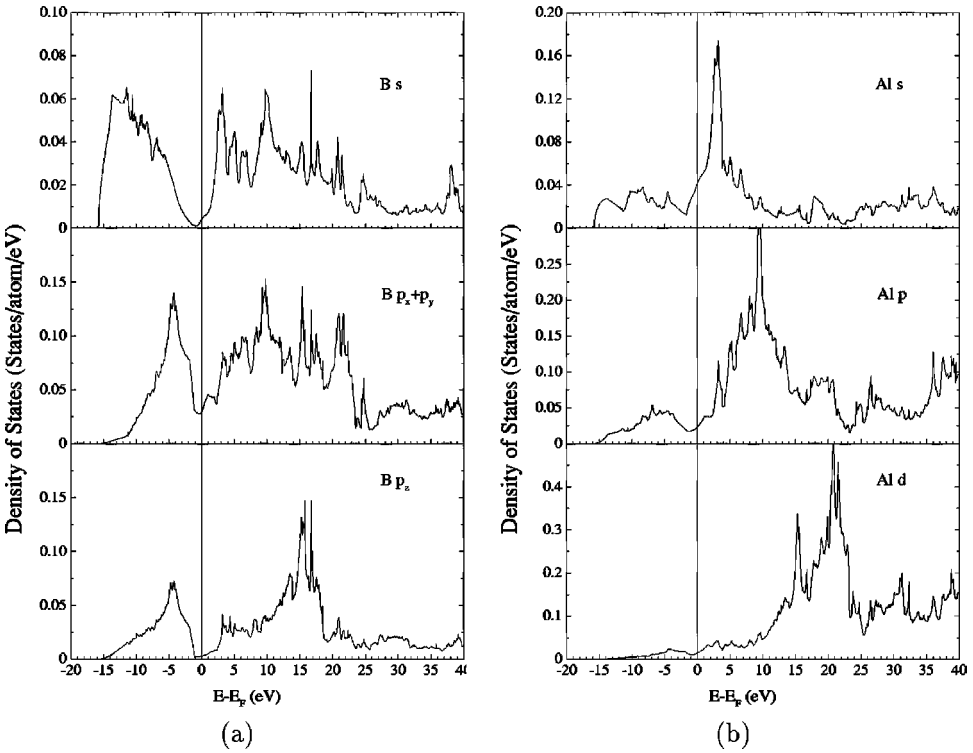

FIG. 2. Calculated symmetry-resolved (ground state) density of states in AlB_2: (a) B site showing the nondegenerate partial *p* states and the *s* states. (b) Al site showing the partial *l* states.

E_F, implying considerable covalency. Higher-energy states 5–20 eV above E_F appear to arise from Ti $4p$ and $5s$ states hybridized with B $2p$ states.

Compared to TiB_2, the electronic structure of AlB_2 has been less studied in the literature. The phase diagram[29] for the Al-B system indicates that aluminum diboride AlB_2 transforms into aluminum dodecaboride AlB_{12} at 980 °C. Band-structure calculations for AlB_2 (using the linear combination of atomic orbitals method)[30] have postulated a charge transfer from Al to B resulting in an effective charge of $Al^{+1.884}$, which is exactly the description proposed by the earlier work of Lipscomb and Britton.[8] These authors claimed that the π bond order between each boron pair in the boron sheet must approach $\frac{2}{3}$ as is the case in isoelectronic benzene. However, we observe from Table II that in hexagonal BN (and graphite) the nearest-neighbor distance within the hexagonal net is about 0.3 Å shorter than the B-B distance in the diboride boron sheet due to the stabilized π bond. This tends to indicate small or insignificant π bonding within the boron sheets in the diborides. Comparing the DOS results for TiB_2 and AlB_2 (Fig. 1), the Al and B unoccupied and occupied DOS's for AlB_2 show a remarkable correspondence, reflecting the strong similarity of these elements as well as the presence of significant amounts of bond covalency or hybridization between the two elements in the AlB_2 structure. The rise of the unoccupied DOS from E_F on both sites is more gradual in the case of AlB_2 relative to TiB_2. Again this is due to the lack of tightly bound d states available for intersheet bonding between the metal and boron hexagonal nets in the AlB_2 structure relative to TiB_2. We also note from Table I that the c/a ratio is smaller in TiB_2 relative AlB_2 due to stronger intersheet bonding. Table III shows the charge decomposition within the spatial division of the unit cell derived from the full potential linearized augmented plane-wave (FLAPW) calculations. When we compare the converged ground-state charge density with that of the simple superposition of neutral atomic charge densities, which is the initial charge density in the Kohn-Sham[31] equations, we find a small charge transfer from the metal to the nonmetal atoms. From Table III we calculate values of 0.24 and 0.28 electrons for TiB_2 and AlB_2, respectively. No pronounced differences between the compounds was apparent and overall substantial covalency is implied. Further, in Fig. 2 we show the site- and symmetry-resolved DOS of AlB_2 (the partial DOS results for TiB_2 was already published in a previous paper[5]). It is interesting to see the close resemblance between the partial B p_z and p_{xy} states in the occupied region, which is a consequence of admixture between in-plane and out of plane B p states. Further Al p and d states hybridize with B p states, producing antibonding states, and give rise to the high-lying peaks observed in the experimental spectra shown in Sec. III C.

Finally, Armstrong *et al.*[30] stated that with respect to B-B bonding, there is little experimental evidence to provide a description of the nature of the bonding in these compounds, as there is little in boron chemistry with which to compare the diborides. This is exactly where orientation dependent ELNES measurements at the B K edge can aid as a quantitative tool in the interpretation of this bonding.

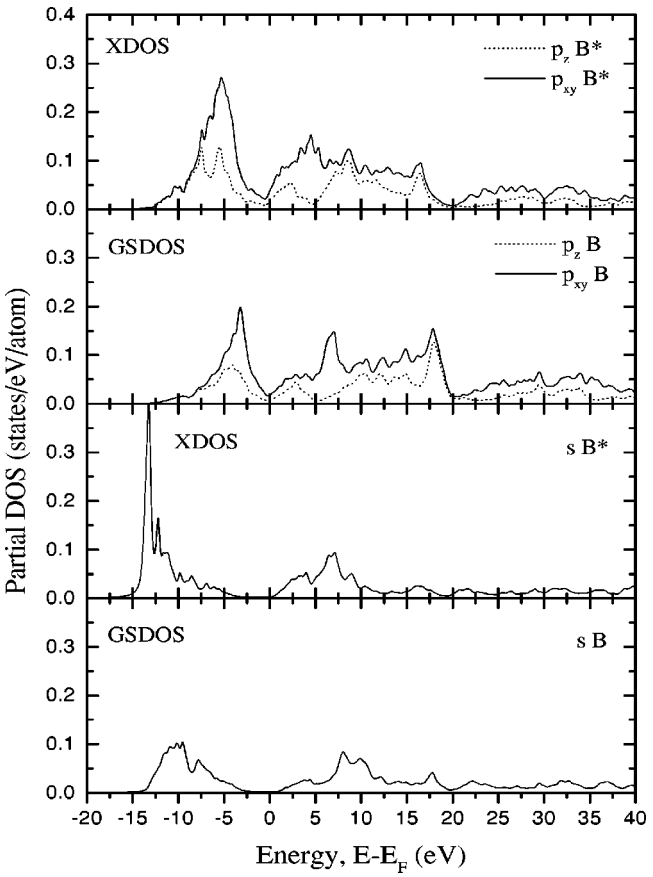

FIG. 3. Local, B-site-projected, partial densities of states for TiB_2 as calculated for the ground state and for the excited state with the presence of the core hole. The core-hole effect is self-consistently accounted for within a $2\times2\times2$ supercell.

B. Results of excited-state calculations showing the influence of the core hole on the DOS

In Fig. 3 we compare the calculated local partial B s, p_z, and p_{xy} DOS curves for ground-state TiB_2 with those found for the final, excited state. In the latter the influence of the core hole was self-consistently accounted for, using the core-excited model. When comparing the ground state DOS and the excited-state DOS (XDOS) we note that the presence of the core hole induces large modifications of the theoretical electronic states. The most interesting effect is the shift of weight toward the bottom of the B bands when a core hole is introduced. In particular the local density of occupied B s states below E_F at a core-ionized site is very different from that of the unperturbed system, with a major peak near the bottom of the band. This effect has also been demonstrated in simulations of corehole effect in light elements (Na, Mg, Al, Si), and transition-metal silicides.[32] We also note that the relative weight of unoccupied B s and p states above E_F is shifted toward lower energy; however, for states higher than 20 eV the difference is less pronounced, due to the large separation of these states from the effectively atomic $1s$ level.

The effect of the core hole on the partial density of B p states shows similar effects to those for the s states. We observe a shift in weight of the major peaks toward lower energy, from the bottom of the valence band to about 20 eV above E_F. It will be shown below that this change induces

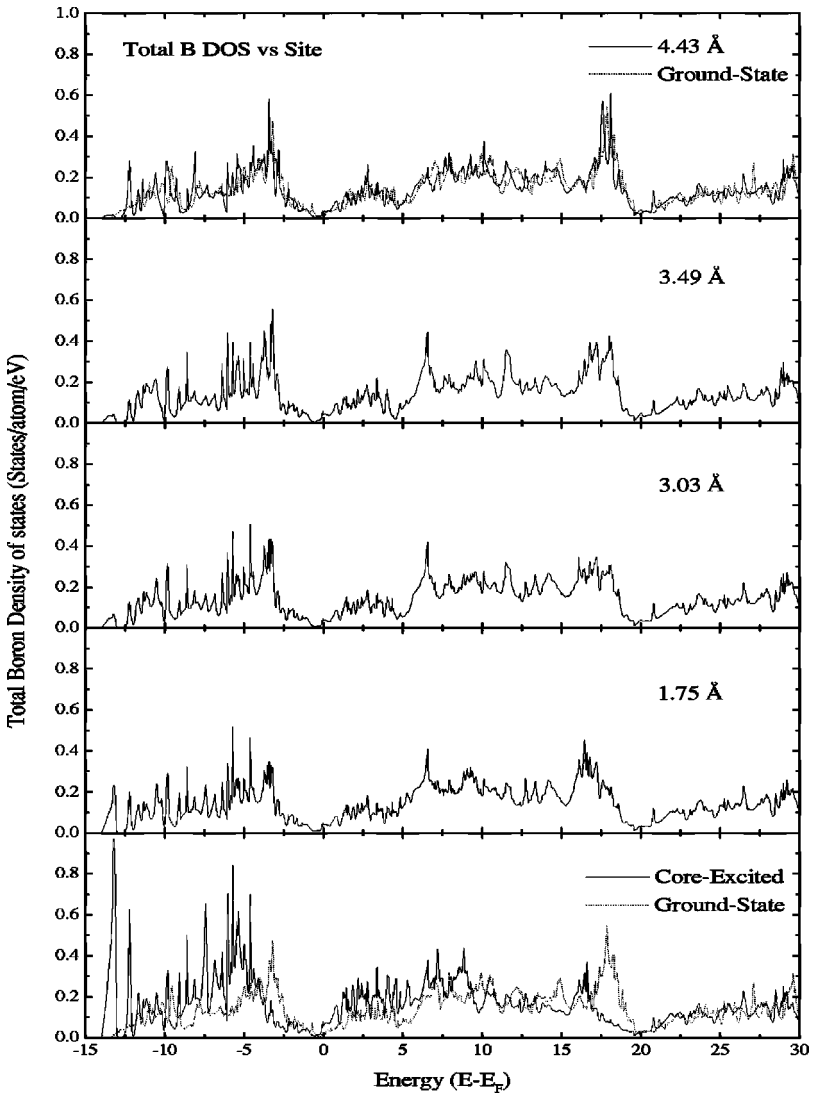

FIG. 4. Total B DOS for TiB_2 at selected sites in the supercell. The distance in Å is relative to the core-excited atom. At the top and bottom of the figure, the ground-state DOS from a $2\times2\times2$ supercell is shown for comparison.

strong changes in the spectral functions, even when lifetime and experimental broadening is taken into account. We also call attention to the increase in the area under the occupied B s, p_z, and p_{xy} states curves below E_F. This corresponds to 0.20, 0.23, and 0.49 extra electrons, respectively, as can be seen from Table III. This reflects the screening of the core hole by the valence electrons which are mainly of B $2s$ and B $2p$ character (see Fig. 1), and is most effective in the B plane. This is in agreement with the momentum resolved experimental spectra (see below), which show enhanced screening of the core hole for electronic transitions perpendicular to c.

In order to investigate the influence of the potential on neighboring atoms, caused by the core-excited atom, we have plotted the projected DOS of different atoms within the supercell (see Fig. 4). The largest modification of the XDOS is naturally found for the atom at the core-hole site. However, for some of the other boron atoms in the supercell there is also a redistribution of the electronic states (similar effects can be seen in Ref. 33 in the case of graphite). For instance, the nearest-neighbor boron atom to the core hole (at a distance of 1.75 Å) has an XDOS which resembles that of the core-hole-excited atom, although with somewhat less pronounced features. As an example we note that the nearest-neighbor atoms have peaks at both -13.2 and -12.2 eV, similar to the excited atom. These peaks have s symmetry as can be seen from Fig. 3, and are modified from being broad states to more localized states in the presence of the core hole. These findings suggest that the core hole is mostly localized on the core-excited atom, but has some weight on the nearest-neighbor atoms, and can be associated with the presence of a Frenkel exciton.[33,34,18] Further, since the perturbation from the ground state is very small at the B site 4.43 Å from the core excited site, this indicates that a $2\times2\times2$ supercell should be large enough to avoid interactions from neighboring supercells in the calculation, which includes a core hole. Thus, to a good approximation, the exciton has both its electron and its hole in a single unit supercell. Naturally, since the hole is localized deep within the core, it is incapable of hopping from one atomic site to another.

In Fig. 5 we compare the $Z+1$ and core-excited approximations for TiB_2. As pointed out by Pickard,[35] the $Z+1$ approximation is less accurate because it attempts to cancel out one of the core electrons by placing an additional charge at the nucleus. In particular there is no distinction between $1s$ and $2p$ core holes in the $Z+1$ approximation. However, for the case of TiB_2, Fig. 5 shows that there is no significant

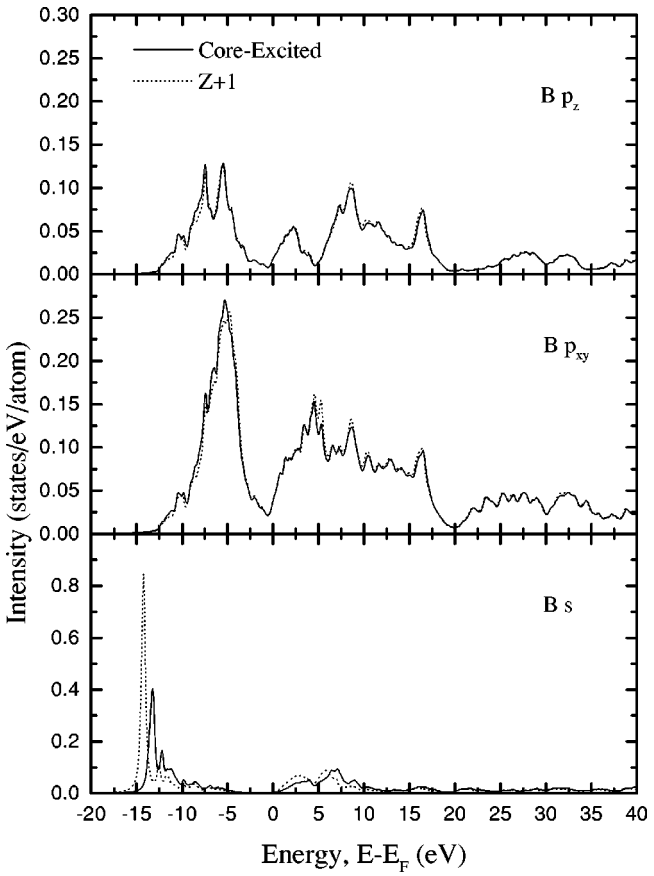

FIG. 5. Comparison of the $Z+1$ and core-excited approximations for the B K edge in TiB_2. In the latter case one of the electrons in the $1s$ orbital was omitted, while the number of electrons in the valence band was increased by one.

difference in the symmetry- and site-resolved B p DOS's derived using the two approximations. These are the states we are probing in our measurements of the B K-edge ELNES. We have obtained similar results for AlB_2. This shows that a deep hole plus an electron is little different from a proton plus an electron, which is acceptable as long as the hole occupies a smaller radius orbit than the electron in the chemical bonds.[36]

C. Comparison of the experimental B *K*-edge spectra with ground- and excited-state calculations

The measured boron K edges of TiB_2 and AlB_2 are shown in Fig. 6. The only dipole allowed transitions from the B $1s$ core level are to final states of p symmetry with a projection at the B site. Therefore we compare the measured spectrum with momentum transfer $\mathbf{q}\|\mathbf{c}$ with the calculated B p_z DOS, and the spectrum with $\mathbf{q}\perp\mathbf{c}$ is compared with B p_x+p_y DOS. The theoretical spectra have been convoluted by a Lorentzian of FWHM of 1 eV, to simulate experimental broadening.

The experimental results in Fig. 6 demonstrate that both TiB_2 and, to a much lesser extent, AlB_2 show some orientation dependency in the B K-edge ELNES. In TiB_2 the most notable feature is the dominance of a peak in the interval 0–5 eV above E_F in the spectra measured with $\mathbf{q}\|\mathbf{c}$. This feature reflects the strong hybridization of Ti $3d$ states with B $2p$ $(2p_z)$, and to a lesser degree B $2s$ states, leading to covalent bonding between the B and Ti sheets. This effect is much less pronounced for the case of AlB_2, presumably due to the absence of available d states in the metal which leads to hybridized Al $2p$ and B $2p$ states being spread out over a much wider energy region. We also note from Fig. 6 [(a) and (b), lower part] that the core-hole potential produces much more dramatic changes just above E_F in AlB_2 compared with TiB_2, which again is an effect of Ti $3d$ states.

In the B K-edge ELNES of both TiB_2 and AlB_2, measured with $\mathbf{q}\perp\mathbf{c}$, the main increase in intensity (relative to $\mathbf{q}\|\mathbf{c}$) arises at around 7 eV and is due to sp^2-hybridized bonding in the plane of the hexagonal B sheets. Again in the case of TiB_2, this σ^* is not greatly influenced by the localized (-5 and 5 eV) unoccupied Ti $3d$ states; however, in AlB_2 the more delocalized Al $2p$ states modify the appearance of this peak significantly. These effects produce the differences in the spectral functions of the diborides studied.

Comparing the experimental spectra of both TiB_2 and AlB_2 with the theoretical calculations, we observe that for

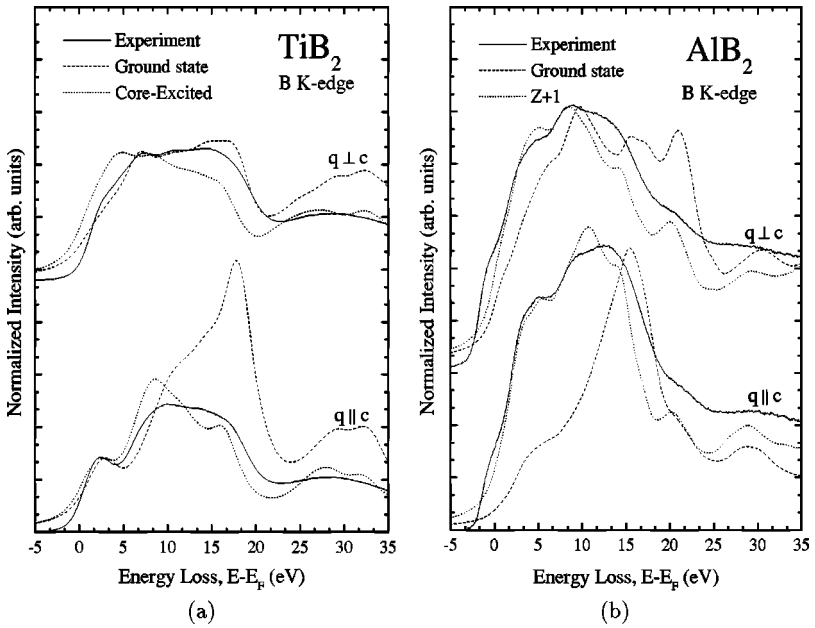

FIG. 6. Symmetry resolved theoretical B K-edge spectra of (a) TiB_2 and (b) AlB_2, with and without the core hole, together with the experimental orientation-resolved spectra for comparison. The core-hole calculations used a 24-atom supercell, and were calculated both within the $Z+1$ approximation and with the core-excited configuration. The experimental data for TiB_2 have been shifted and aligned with the calculated ground-state spectrum, while for AlB_2 the experimental data have been aligned with calculated spectrum using the $Z+1$ approximation for the core hole.

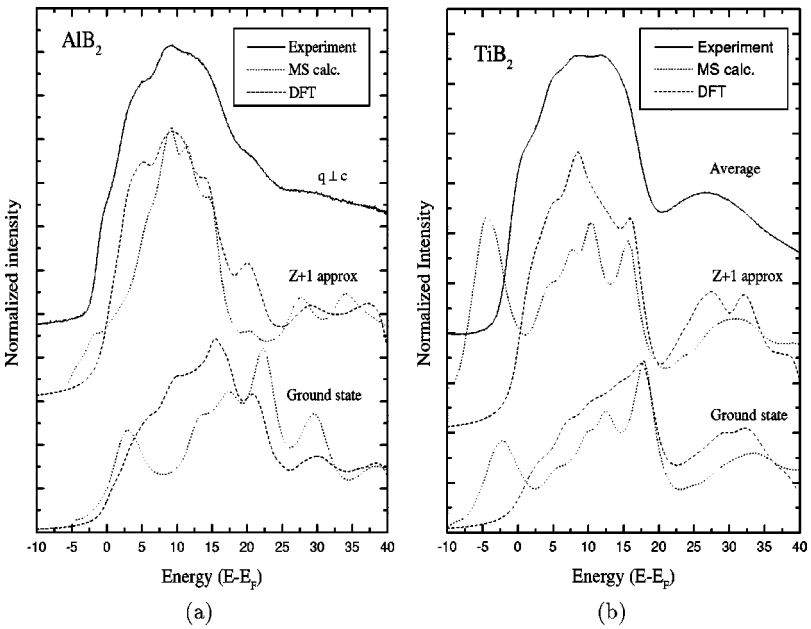

FIG. 7. Comparison of the experimental B *K*-edge ELNES spectrum in (a) AlB_2 $\mathbf{q}\perp\mathbf{c}$ and (b) TiB_2 (average) with the results of eight-shell MS calculations and with the boron *p* DOS derived from the LAPW calculation. Both the ground state and $Z+1$ approximations are compared.

spectra with $\mathbf{q}\|\mathbf{c}$, satisfactory agreement with the calculated B $2p_z$ states is only achieved after proper inclusion of the core hole using the core-excited approximation. We propose that this effect arises since the valence electrons in this direction, arising from the covalent intersheet bonding, are more tightly bound and thus unable one to screen the exposed potential due to the core hole. Conversely, for spectra measured with $\mathbf{q}\perp\mathbf{c}$, the effect on the *p* DOS of the inclusion of the core hole is much less pronounced and, in the case of TiB_2, is perhaps an overestimate when compared to the experimental result. The latter observation must be due to the increased screening in a direction along the B sheets ($\mathbf{q}\perp\mathbf{c}$) due to the more mobile valence electrons. These effects can also be seen in the data in Table III, where inclusion of the core hole leads to an increase in the occupied B p_z and B $p_{x,y}$ DOS's of 0.23 and 0.49 electrons, respectively, clearly the screening occurs more readily perpendicular to *c* axis (*z* direction). Overall, when proper inclusion of the core-hole effects is undertaken, we observe good agreement between theory and experiment for both TiB_2 and AlB_2.

In Fig. 7 we compare the results of the multiple-scattering calculations with those derived using the FLAPW method. In the MS approach the calculation is averaged over all orientations of the scattering vector and compared with total *p* DOS from the band method. The MS calculations of the B *K*-edge ELNES in the two diborides were carried out using a cluster of eight shells (the total number of atoms is 92). Convergence was assured by comparing with the results obtained using six- and seven-shell clusters. As we can see in Fig. 7, overall the LAPW band method gives a substantially better agreement with experiment. However in the case of AlB_2, the MS approach with the $Z+1$ approximation for the core hole shows satisfactory agreement with experiment. This is not the case for TiB_2 which is probably due to the imperfection of the simple muffin-tin approximation employed in the MS calculations. This spherical symmetry of the potential is a poor approximation for the highly directional *p*-*d* bonding between boron and titanium in TiB_2, which is apparent in the orientation-dependent measurements.

IV. CONCLUSIONS

In this work we have presented the B *K*-edge ELNES spectra of the isostructural compounds AlB_2 and TiB_2, as well as the orientation dependence of such spectra. Experimental results have been compared to the results of theoretical FLAPW calculations of the DOS which imply substantial covalency in the bonding.

The orientation dependence of the spectra for both compounds may be understood from the highly anisotropic layered structure. In particular, TiB_2 shows strong anisotropy in the electronic structure, reflecting the strong intersheet bonding arising from hybridization between the Ti $3d$ and B $2p$ states. In AlB_2 there is also substantial covalent intersheet bonding; however, owing to the tightly bound *d* states, less directionality is observed.

Further we observe significant differences between the ground-state symmetry-resolved DOS calculations and experimental orientation dependent B *K*-edge ELNES data for both AlB_2 and TiB_2. By introducing a $1s$ core hole at the boron site and carrying out self-consistent calculations within a supercell approach, we find that we can properly describe the changes in spectral weight induced by the core hole, particularly for the spectrum measured with momentum transfer parallel to *c*, where we expect there to be reduced screening due to the presence of strong intersheet covalent bonding.

ACKNOWLEDGMENTS

The authors are grateful to the Norwegian Research Council for financial support. We acknowledge Gunnar Pettersen, NTNU, for providing the sintered TiB_2 specimen, and Lars Arnberg for the Al-3% B alloy; Peter Blaha, Technical University-Wien, for help and information on the WIEN97 program and Jørn Amundsen for help and support on the parallel machine CRAY T3E.

[1] J. C. Fuggle, in *Unoccupied Electronic States*, edited by J. C. Fuggle and J. E. Inglesfield (Springer-Verlag, Berlin, 1992).
[2] J. Zaanen *et al.*, Phys. Rev. B **32**, 4905 (1985).
[3] R. D. Leapman, R. A. Grunes, and P. L. Fejes, Phys. Rev. B **26**, 614 (1982).
[4] B. T. Thole *et al.*, Phys. Rev. B **32**, 5107 (1985).
[5] K. Lie, R. Brydson, and H. Davock, Phys. Rev. B **59**, 5361 (1999).
[6] H. J. Davock *et al.*, in *Proceedings of EMAG97*, edited by F. M. Rodenburg, Inst. Phys. Conf. Proc. No. 153 (Institute of Physics and Physical Society, Cambridge, 1997), pp. 609–612.
[7] M. I. Matkovich, G. V. Samsonov, P. Hagenmuller, and T. Lundstrom, in *Boron and Refractory Borides*, edited by M. I. Matkovich (Springer-Verlag, Berlin, 1977).
[8] W. N. Lipscomb and D. Britton, J. Chem. Phys. **33**, 275 (1960).
[9] D. C. Tian and X. B. Wang, J. Phys.: Condens. Matter **4**, 8765 (1992).
[10] X. B. Wang, D. C. Tian, and L. L. Wang, J. Phys.: Condens. Matter **6**, 10 185 (1994).
[11] N. D. Browning, J. Yuan, and L. M. Brown, Ultramicroscopy **38**, 291 (1991).
[12] G. Pettersen, Ph.D. thesis, Norwegian University of Science and Technology, 1997.
[13] L. A. J. Garvie, A. J. Craven, and R. Brydson, Am. Mineral. **80**, 1132 (1995).
[14] R. F. Egerton, *EELS in the Electron Microscope* (Plenum, New York, 1996).
[15] C. B. Boothroyd, K. Sato, and K. Yamada, in *Proceedings of the 7th International Conference for Electron Microscopy*, edited by L. O. Peachey and D. B. Williams (San Francisco Press, San Francisco, 1990), Vol. 2, p. 80.
[16] P. Blaha, K. Schwarz, P. Dufek, and R. Augustyn, WIEN97, *A Full Potential Linearized Augmented Plane Wave Package for Calculating Crystal Properties* (Karlheinz Schwarz, Techn. Univ. Wien, Vienna, 1999). ISBN 3-9501031-0-4, updated version of P. Blaha, K. Schwarz, P. Sorantin, and S. B. Trickey, Comput. Phys. Commun. **59**, 399 (1990).
[17] P. E. Blöchl, O. Jepsen, and O. K. Anderson, Phys. Rev. B **49**, 16 223 (1994).
[18] H. P. Hjalmarson, H. Büttner, and J. D. Dow, Phys. Rev. B **24**, 6010 (1981).
[19] P. J. Durham, J. B. Pendry, and C. H. Hodges, Comput. Phys. Commun. **25**, 193 (1982).
[20] D. D. Vvedensky, D. K. Saldin, and J. B. Pendry, Comput. Phys. Commun. **40**, 421 (1986).
[21] X. Weng, P. Rez, and H. Ma, Phys. Rev. B **40**, 4175 (1989).
[22] K. Schwarz, Phys. Rev. B **5**, 2466 (1972).
[23] H. Ihara, M. Hirabayashi, and H. Nakagawa, Phys. Rev. B **16**, 726 (1977).
[24] J. K. Burdett, E. Canadell, and G. J. Miller, J. Am. Chem. Soc. **108**, 6561 (1986).
[25] A. L. Ivanovsky, N. I. Medvedeva, and J. E. Medvedeva, Mendeleev Commun. **4**, 129 (1998).
[26] G. P. Shveikin and A. L. Ivanovkii, Russ. Chem. Rev. **63**, 711 (1994).
[27] V. M. Anishcik and N. N. Dorozhkin, Phys. Status Solidi B **160**, 173 (1990).
[28] A. Pasturel, C. Colinet, and P. Hichter, Physica B **132**, 177 (1985).
[29] O. N. Carlsson, in *Binary Alloy Phase Diagrams, 123*, edited by T. B. Massalski (ASM International, Ohio, 1990).
[30] D. R. Armstrong, A. Breeze, and P. G. Perkins, J. Chem. Soc., Faraday Trans. **7**, 952 (1977).
[31] W. Kohn and L. J. Sham, Phys. Rev. **140**, A1133 (1965).
[32] P. J. W. Weijs *et al.*, Phys. Rev. B **41**, 11 899 (1990).
[33] R. Ahuja *et al.*, Phys. Rev. B **54**, 14 396 (1996).
[34] C. Kittel, *Introduction to Solid State Physics* (Wiley, New York, 1986).
[35] C. J. Pickard, Ph.D. thesis, University of Cambridge, 1997.
[36] W. A. Harrison, in *Festkorperprobleme*, edited by J. Treusch (Vieweg., Wiesbaden, 1977), Vol. 17, p. 135.